Thermal conductivity and diffusivity of triple-cation perovskite halide materials for solar cells

Zhelu Hu, Lionel Aigouy, Zhuoying Chen, Danièle Fournier

Thermal conductivity and diffusivity of triple-cation perovskite halide materials for solar cells

Zhelu Hu,[1] Lionel Aigouy,[1,a)] Zhuoying Chen,[1] Danièle Fournier[2]

[1]*LPEM, ESPCI Paris, PSL Research University, Sorbonne Universités, CNRS, 10 rue Vauquelin, 75005 Paris, France*

[2]*Sorbonne Université, CNRS, Institut des NanoSciences de Paris, UMR 7588 F-75252, Paris, France*

We report on the measurement of the thermal conductivity and the thermal diffusivity by the technique of modulated thermoreflectance microscopy on a mixed-cation perovskite material [$Cs_{0.05}$(formamidinium$_{0.83}$methylammonium$_{0.17}$)$_{0.95}$Pb($I_{0.83}Br_{0.17}$)$_3$] widely applied for solution-processed perovskite solar cells. Such materials are supposed to present an improved thermal stability compared to methylammonium-based single cation perovskites. Our measurements are performed on perovskite/TiO_2/SnO_2:F/SiO_2 structures, with perovskite thicknesses ranging between 250 nm and 1000 nm. This configuration is the one of a real solar cell, with the same substrate and intermediate layers than an operating device. We measured a thermal conductivity k_{per} of 0.26 ± 0.03 W m^{-1} K^{-1} and a thermal diffusivity D_{per} of 3.5×10^{-7} ± 0.5 m^2 s^{-1}. The value for the thermal conductivity is comparable to the one measured on single cation perovskites which is generally in the 0.2-0.6 range. The value for the thermal diffusivity was not reported previously.

I. INTRODUCTION

Hybrid metal-halide perovskites form a family of highly promising materials for the development of future-generation solar cells.[1] Their interesting physical properties, such as a direct bandgap, a high absorption coefficient, and a high charge carrier mobility, make them able to reach a photo-voltaic efficiency larger than 25%.[2-8] These cells are inexpensive to produce, the compounds that compose them are abundant, the temperature fabrication is low, and the chemical techniques to manufacture them are adaptable on a large scale. Their main drawback

a) Electronic mail: lionel.aigouy@espci.fr

comes from their stability over time, which limits their current development. These materials are very sensitive to humidity, ultraviolet light and temperature rises.[9,10] In particular, during their operation in front of the sunlight, the temperature of the cells can increase, causing an accelerated degradation. This is very problematic for methylammonium (MA)-based perovskites which appears to be thermally unstable[11] and that can degrade above ~358 K[8]. Recently, it has been observed that formamidinium (FA)-based cells exhibit a much larger stability than MA-based ones, making this compound very promising for future developments.[10] Yet FA-based perovskite halides suffer from the formation of amorphous phases at some I/Br ratio, the tuning of which is an efficient tool to modify the bandgap of the material. The addition of Cs^+ cation into the formulation and the formation of the triple mixed cation (MA-FA-Cs) perovskite halides can largely overcome the formation of amorphous phases facilitating a continuous tuning of bandgap by tuning the I/Br ratio while keeping the interesting thermal stability.[8]

In this article, we have studied the thermal properties of triple mixed cation FA-MA-Cs-based perovskite solar cells.[4,5,9] More specifically, we have measured both their thermal conductivity and thermal diffusivity which are crucial parameters to predict how fast and how efficiently heat will dissipate in the active layer and toward the substrate. While several thermal conductivity measurements have already been performed on MA-based compounds, very little data is available on triple-cation-based ones. Our measurements indicate that the thermal conductivity of such compounds is only slightly smaller than the one of MA-based perovskites found in literature, showing that the substitution of MA^+ by FA^+ and Cs^+ has a very limited influence on the thermal properties of these compounds. The experiments were carried out by modulated thermoreflectance microscopy (MTRM) on $Cs_{0.05(}(FA_{0.83}MA_{0.17})_{0.95}Pb(I_{0.83}Br_{0.17})_3$ layers of different thicknesses and directly grown on a TiO_2/SnO_2:F/SiO_2 substrate, in a real solar cell

configuration. The relative concentration of FA, MA and Cs was chosen to optimize the power conversion efficiency, the morphology of the grains and their stability.

II. Experimental details

The structure of the cells is illustrated in Fig. 1(a). A 50 nm-thick planar compact TiO_2 electron transport layer (ETL) was deposited by spin coating on fluorine-doped tin oxide (SnO_2:F or FTO) coated SiO_2 substrates of 500 nm thickness. Crystalline $Cs_{0.05(}(FA_{0.83}MA_{0.17})_{0.95}Pb(I_{0.83}Br_{0.17})_3$ was then deposited by spin-coating on the substrate under different concentration and speed and five films were grown with perovskite thicknesses t_{per} equal to 250, 310, 400, 540 and 1000 nm respectively (see the supplementary materials for more information about the synthesis). We show in Fig. 1(b) and 1(c) a cross-sectional and in-plane scanning electron microscope (SEM) images of the 540 nm-thick perovskite surface. The size of the grains lies in the 100-300 nm range, in agreement with previous measurements performed on FA- and MA-based structures.[8,12,13] A similar morphology and grain size was observed on the samples that have a smaller or larger perovskite thickness (see supporting information). Details about the composition of the perovskite layers, obtained from X-rays diffraction (XRD) and energy dispersive X-ray spectroscopy (EDX) are also given in the supporting information. Finally, a 150 nm-thick gold film was then deposited on the perovskite layers for the thermal measurements.

MTRM measurements were carried out in a homemade optical microscope[14,15] whose principle is described in Fig. 1(d). A modulated pump beam (λ = 532 nm, P = 2 mW/μm^2) is focused on the sample surface on a ~1 µm size spot and heats the Au film locally and periodically (frequency f = 50-800 kHz). A CW probe beam (λ = 488 nm, P = 100 µW/μm^2) is also focused on the surface

in a similar way. The heat created by the pump beam then diffuses laterally on the surface (r direction) and inside the different layers (z direction). This induces a periodic modulation of the surface temperature of the Au layer and then a periodic modulation of the Au reflection coefficient ΔR. The probe beam is detected by a silicon detector whose output is sent to a lock-in amplifier which can extract the amplitude ΔR and the phase $\Delta\phi$ of the modulated photoreflectance signal. During an experiment, the pump beam is progressively moved away from the probe beam, and ΔR and $\Delta\phi$ are measured as a function of their separation distance.

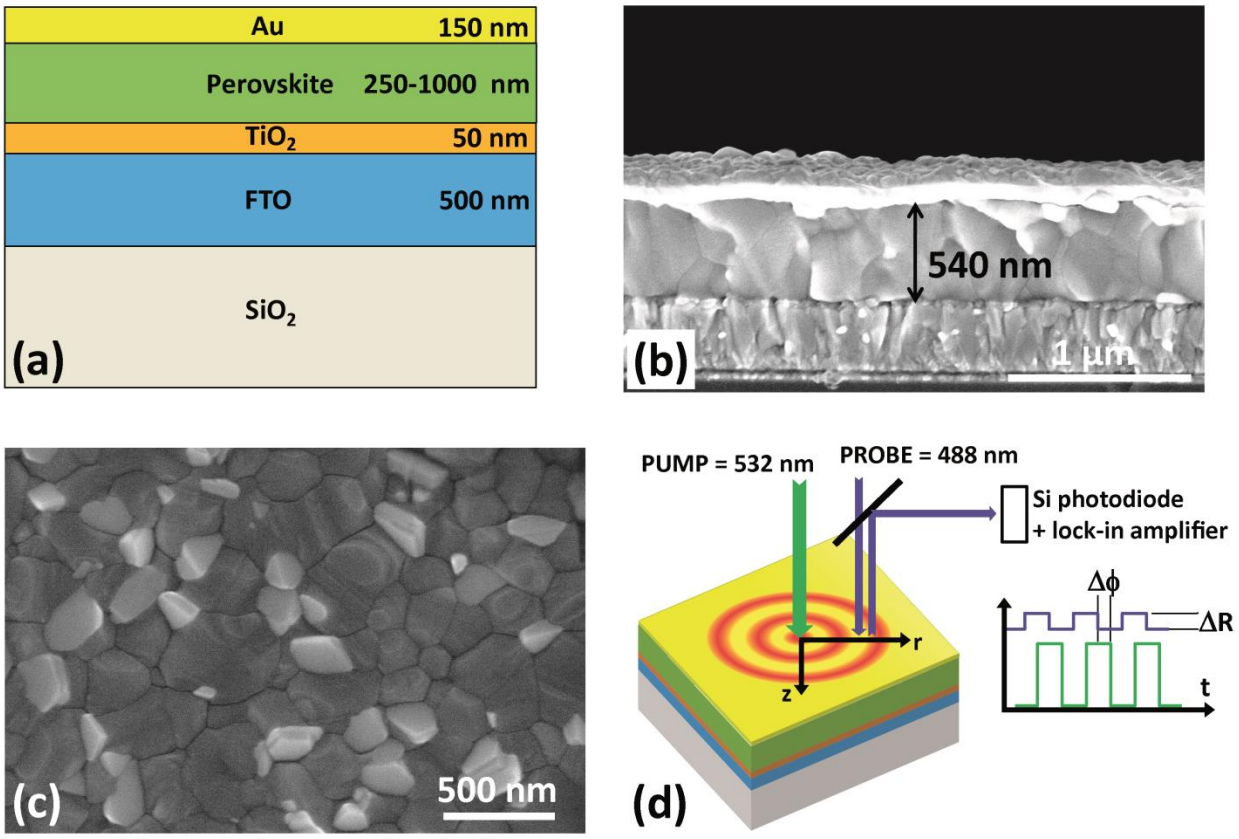

Figure 1: sketch of the solar cell structure (a), cross-sectional SEM image of the 540-nm thick perovskite structure (b), SEM image of the surface of perovskite prior to Au deposition (c), and sketch of the modulated photoreflectance experimental set-up (d).

III. Results and discussion

To extract the thermal conductivity *k* and diffusivity *D* of the different layers in the structure, we used a thermal model similar to the one described in ref. 15. Both ΔR and $\Delta\phi$ decrease as the distance between the two beams increases and the slopes of the curves are a function of *k* and *D* of the stack. Due to the circular symmetry of the pump laser spot on the surface, the heat diffusion equation is solved in cylindrical geometry using a Hankel transformation method. Here, we have to deal with several intermediate materials and layers (SiO_2, FTO, TiO_2, Au) whose thermal properties are usually known in the absolute in their bulk form but are in fact strongly dependent on the deposition conditions. We therefore performed a progressive analysis and first characterized the properties of the Au layer on the raw SiO_2 substrate by removing the FTO. Then, we successively studied the SiO_2/FTO/Au and the SiO_2/FTO/TiO_2/Au structures to extract the FTO and the TiO_2 thermal properties respectively. This layer by layer procedure minimizes the uncertainty on each material. The measured thermal conductivity *k* and thermal diffusivity *D* of Au, FTO and TiO_2 are summarized in Table I. No dependence on the excitation power was observed for these parameters during the experiments. The values are in reasonable agreement with the ones found in literature.[16-19]

TABLE I. Thermal parameters of the different underlying materials involved.

Material	SiO_2	Au	FTO	TiO_2
k ($W\ m^{-1}\ K^{-1}$)	1.12	220	39	10
D ($10^{-7}\ m^2\ s^{-1}$)	6.13	880	150	36

For TiO_2, we found a thermal conductivity value close to the one of the bulk. In fact, due to its small thickness, the influence of the TiO_2 layer is very weak and smaller values could have been used for fitting the data. Once all the sublayers were characterized, we then studied the entire cells which contain the mixed FA-MA perovskite. We followed the approach described in ref 15 in the case of lithium phosphorous oxynitrile films grown on a Si substrate. This methodology consists to first study the structures at high frequency (800 kHz) and then at low frequency (100 kHz). By varying the modulation frequency we change the thermal penetration depth. In that case, at 800 kHz, we can fit the experiment without taking into account the thickness of the perovskite layer which can be considered as infinite from a thermal point of view. When lowering the frequency and/or the thickness of the layer, the lower interface is reached by heat and the simulations have to take into account the interface perovskite/TiO_2.

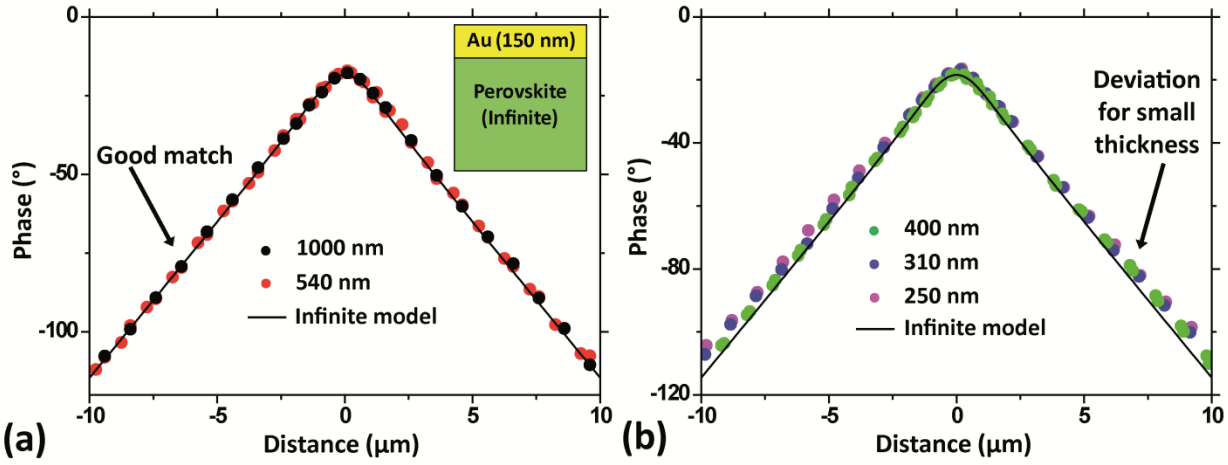

Figure 2: Phase of the MTRM signal for t_{per} = 1000 nm and 540 nm (a) and for t_{per} = 400 nm, 310 nm, and 250 nm (b). On both graphs, the black curve represents a simulation with an infinite model.

We show in Fig. 2 the phase of the MTRM signal measured at high frequency (800 kHz) for all five thicknesses. Same curves were measured at different positions on the surface and in different directions, which shows a good uniformity and a weak sensitivity to an eventual anisotropy of the films. Note that the crystallites may be oriented differently from each other, but the measurement is averaged over the size of the laser spot. As seen in Fig. 2(a), the experimental curves for t_{per} = 1 µm and t_{per} = 540 nm are superimposed. For this thickness range, this means that, at this frequency, the thickness of perovskite is not a parameter that influences heat diffusion. Perovskite is not a very good thermal conductor and heat does not reach the lower interface, and the structure behaves like an infinite material. Using an infinite model, we fitted the experimental data and found approximate values for the thermal conductivity and diffusivity of the perovskite layer: k_{per} = 0.22 W m^{-1} K^{-1} and D_{per} = 3×10^{-7} m^2 s^{-1}. Interestingly, for smaller thicknesses [see Fig. 2(b)], the infinite model does not fit anymore the experimental data. For these structures, heat reaches the interface between the perovskite and TiO_2, and the substrate cannot be neglected anymore. This enables us to have an idea of the thermal diffusion length μ which is given by $\mu = \sqrt{D/\pi f}$ where D and f are the thermal diffusivity and the frequency respectively. For D = 3×10^{-7} m^2 s^{-1} and f = 800 kHz, we find μ = 345 nm, a value which is consistent with the thickness of the perovskite layer below which the substrate cannot be ignored anymore. Another parameter we can extract from the fit of Fig. 2(a) is the thermal effusivity e of the perovskite layer which characterizes its ability to exchange thermal energy with its surroundings. Knowing that $e = k/\sqrt{D}$, we find e = 400 W m^{-2} K^{-1} s$^{1/2}$ which is a value similar to the one of a thermal insulator like wood and much smaller than the ones of metals.

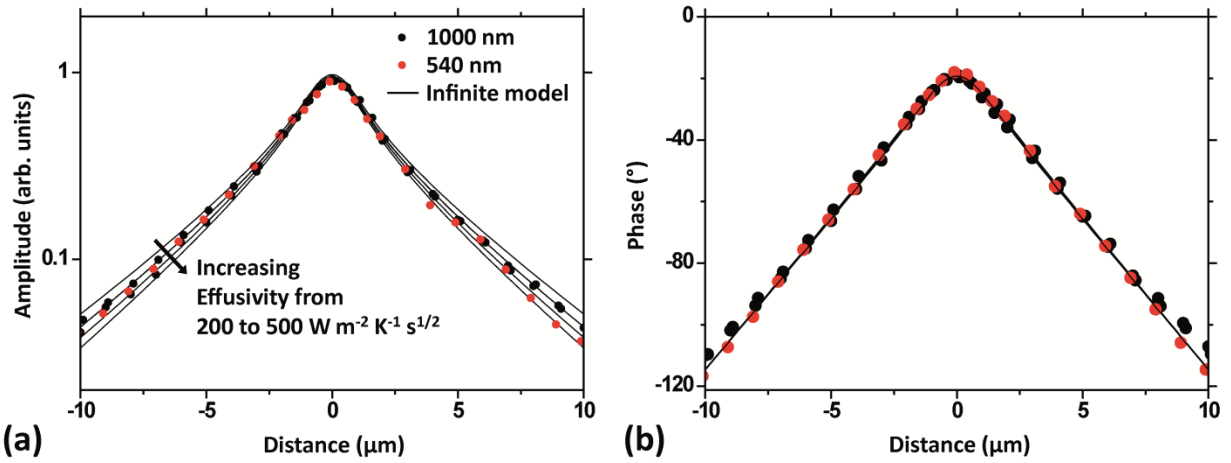

Figure 3: Amplitude (a) and Phase (b) of the MTRM signal for t_{per} = 1000 nm and 540 nm for different values of the effusivity. Circles: experimental values; lines: simulations considering an infinite model with e = 200, 300, 400, 500 W m^{-2} K^{-1} $s^{1/2}$.

However, knowing the thermal effusivity does not allow to find *D* and *k*. The coupled parameters *D* and *k* are unfortunately not unique and good fits can also be obtained for slightly different values. An example showing the influence of *k* on the phase of the simulated curves for t_{per} = 1 µm and t_{per} = 540 nm is presented in Fig.3. Setting $D = 4\times10^{-7}$ m^2 s^{-1} and varying *k* from 0.12 to 0.31 W m^{-1} K^{-1}, which corresponds to a variation of the effusivity between 200 and 500 W m^{-2} $K^{-1}s^{1/2}$, does not modify the simulated phase. The corresponding simulated amplitude ΔR slightly differs but the changes are not important enough to diminish the uncertainty of this measurement. To accurately determine the best values of *D* and *k*, we need to fit the data at smaller frequencies and on all the structures simultaneously. The thermal diffusion length μ increases with decreasing frequency (it varies like the square root of 1/*f*). For instance, μ is supposed to be a factor $\sqrt{8}$ larger at 100 kHz than at 800 kHz. In that case, the lower interfaces

influence the MTRM signals and we cannot use anymore the semi-infinite model, we need to take into account the interfaces of all the materials present in the cell.

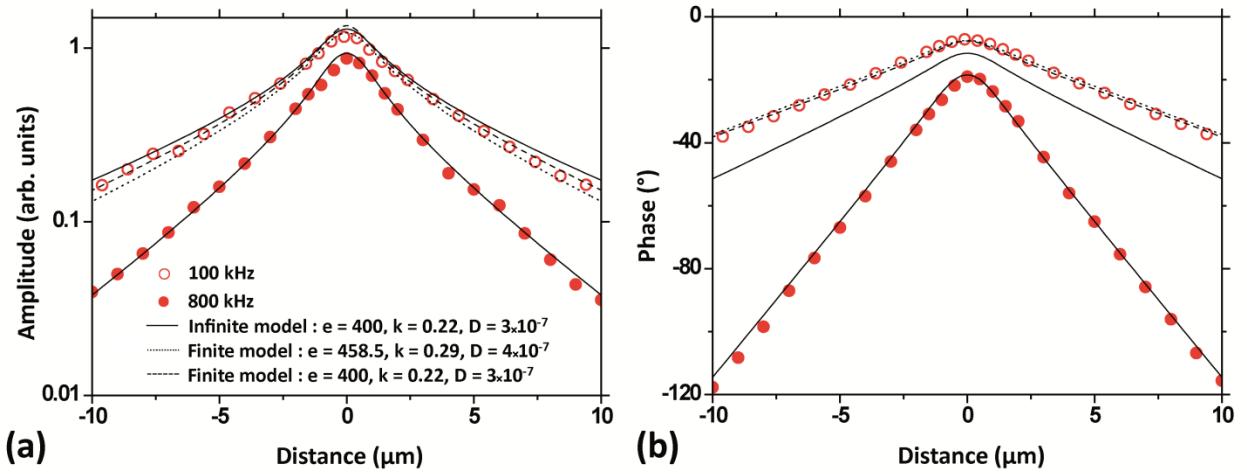

Figure 4: Amplitude (a) and Phase (b) of the MTRM signal for t_{per} = 540 nm at 100 kHz and 800 kHz. Circles: experimental data. Lines: simulation with an infinite model (full lines) or with a finite model (dashed and dotted lines).

We first focused on the sample of intermediate thickness (t_{per} = 540 nm). The experimentally measured amplitude and phase of the MTRM signal are represented in Fig. 4 for two frequencies: 800 kHz (full red circles) and 100 kHz (thin red circles). Due to the larger diffusion length, the amplitude and phase measured at 100 kHz decrease more slowly than the 800 kHz ones. The infinite model (full lines), which describes well the experimental data at 800 kHz is no more accurate at 100 kHz, in particular on the phase which decreases too fast. A much better agreement is obtained with a model which takes into account the thickness of the layer, the interfaces and the different materials of the structure.[15] Good fits can be obtained for the couples of values k_{per} = 0.29 W m^{-1} K^{-1} / D_{per} = 4×10^{-7} m^2 s^{-1} which gives an effusivity e = 400 W m^{-2} K^{-1} s$^{1/2}$ and k_{per} = 0.22 W m^{-1} K^{-1} / D_{per} = 3×10^{-7} m^2 s^{-1} which gives e = 458.5 W m^{-2} K^{-1} s$^{1/2}$. For

both couples of values, the phase variations are the same, but the amplitude is slightly different. From these fits, we now have a reasonable approximation of the value of the thermal conductivity and diffusivity of the perovskite material. In addition to the experiment on the 540 nm-thick sample, we checked and improved the accuracy of these values on thinner samples and at several frequencies between 50 kHz and 800 kHz.

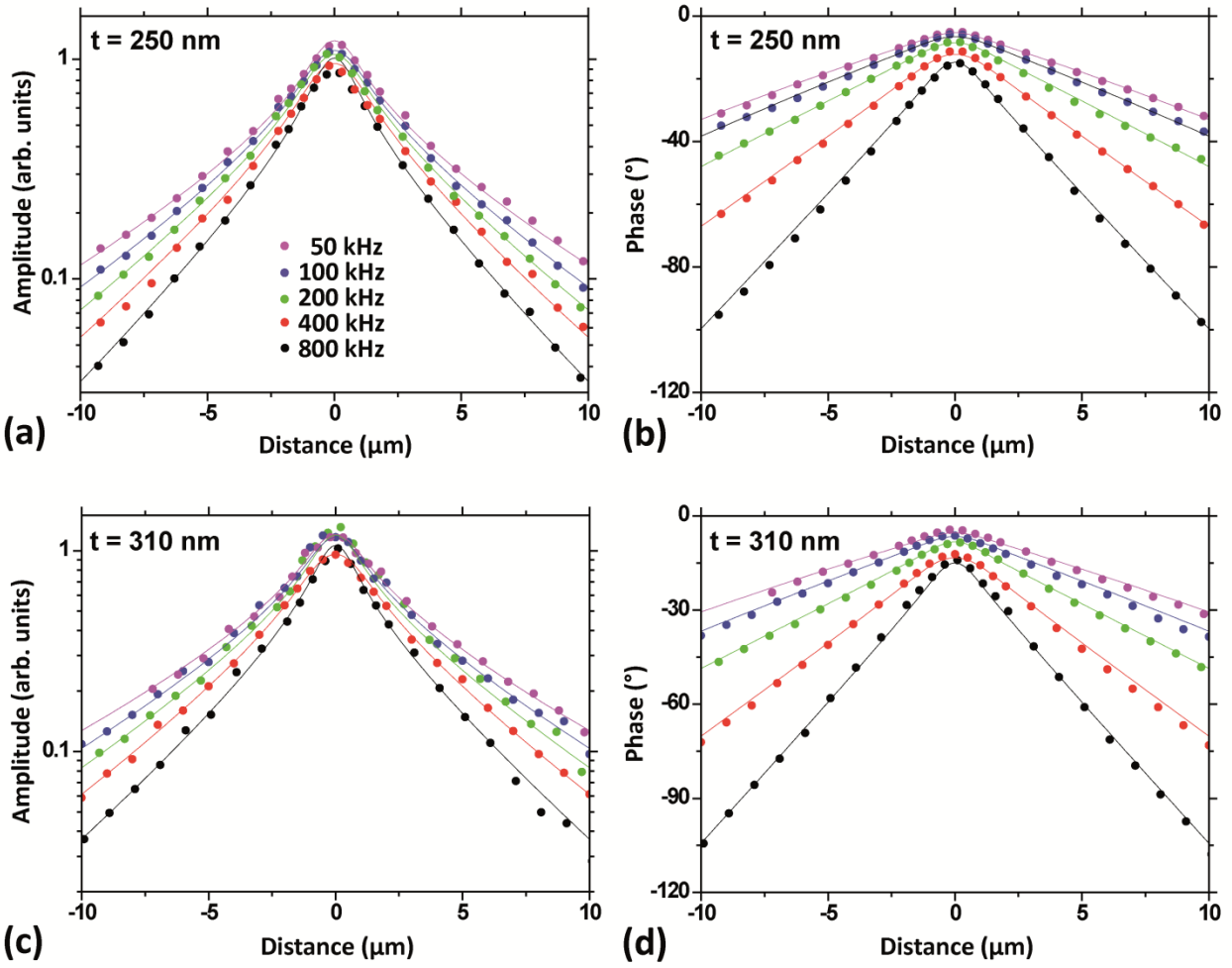

Figure 5: Amplitude (a,c) and phase (b,d) of the MTRM signal for t_{per} = 250 nm and 310 nm, at 5 different frequencies. Full circles: experimental data, full lines: simulations with a finite model (k_{per} = 0.26 W m^{-1} K^{-1} D_{per} = 3.5×10^{-7} m^2 s^{-1} e = 439 W m^{-2} K^{-1} s$^{1/2}$).

We show in Fig. 5 the MTRM experiments carried out on 250 nm and 310 nm thick samples at five frequencies from 50 kHz to 800 kHz. The best agreement was found for k_{per} = 0.26 W m^{-1} K^{-1} and D_{per} = 3.5×10^{-7} m^2 s^{-1} which gives an effusivity e = 439 W m^{-2} K^{-1} $s^{1/2}$. The uncertainty was estimated to 0.03 W.m^{-1}.K^{-1} for k and 0.5×10^{-7} m^2 s^{-1} for D. Let us now compare the measured thermal conductivity to the values found in literature on similar thin film or bulk samples. As summarized in Table II, most of the available data concern MA-based perovskites, not the mixed cation ones. Apart from the results given in ref. 23, all thermal conductivities are found to be between 0.2 and 0.7. In our case, we find a value in the same range, showing that the incorporation of Cs and FA does not change the thermal properties compared to MA-based compounds.

Our measurements were performed on a series of samples of variable thickness without considering that k was thickness-dependent. We think this assumption is valid because the thinnest perovskite layer (250 nm) is not small enough to influence the scattering of phonons, whose mean free path is much smaller than the thickness of the polycrystalline perovskite layer.[27] In addition, Heiderhoff et al[22], observed that the thermal conductivity of several perovskite materials was nearly identical between the bulk and a 200 nm thin film. Finally, we observed by SEM that the perovskite layers were very similar for all samples, the size of the grains being nearly identical, which presumably discard the influence of the morphology on the materials thermal properties (see supplementary materials). Regarding the thermal diffusivity, we could not find a value for similar compounds in the literature to make a comparison. However, k and D are linked through the simple relation $k/D = \rho C$ where ρ is the density and C is the specific heat. The density of our material is not well known but since its molar mass (611.23 g/mol) is approximately the same than the one of $CH_3NH_3PbI_3$ (619.9 g/mol) we can speculate

reasonably both materials have similar densities $\rho \sim 4000$ kg/m^3.[28] From the previous relation, we can deduce the specific heat $C = 113.5$ J.K^{-1}.mol^{-1}, which is of the same order of magnitude than the one found in literature for many similar compounds ($C = 170 - 190$ J K^{-1} mol^{-1} for (MA)PbBr$_3$ and (MA)PbI$_3$ in ref. 29) thus confirming the accuracy of our values for k and D.

TABLE II. Room temperature thermal conductivities of some MA- and FA-based perovskite materials.

Material		k (W m^{-1} K^{-1})	Reference
Cs(FA,MA)Pb(IBr)$_3$	Thin film	0.26 ± 0.03	This work
$CH_3NH_3PbI_3$	Polycrystalline	0.3	Pisoni et al. [20]
$CH_3NH_3PbI_3$	Thin film	0.2-0.5	Guo et al. [21]
$CH_3NH_3PbI_3$	Thin film	0.33 ± 0.12	Heiderhoff et al. [22]
$CH_3NH_3PbBr_3$	Thin film	0.39 ± 0.05	Heiderhoff et al. [22]
$CH_3NH_3PbCl_3$	Thin film	0.50 ± 0.12	Heiderhoff et al. [22]
$CH_3NH_3PbI_3$	Thin film	11.2 ± 0.8	Chen et al. [23]
$CH_3NH_3PbI_3$	Polycrystalline	0.6	Kovalsky et al. [24]
$CH_3NH_3PbI_3$	Polycrystalline	0.6-0.7	Kovalsky et al. [25]
$CH_3NH_3PbI_3$	Nanowire	0.23	Wang et al. [26]
$CH_3NH_3PbBr_3$	Nanowire	0.3-0.35	Wang et al. [26]

IV. Conclusions

In summary, we have measured by modulated thermoreflectance microscopy the thermal conductivity and thermal diffusivity of a recently developed mixed cation perovskite material, whose thermal stability is supposed to be improved compared to MA-based single cation perovskites. Our measurements were performed on a series of structures of variable thicknesses, of same morphologies, which strengthen the validity of our study. The value found for the thermal conductivity ($k_{per} = 0.26$ W m^{-1} K^{-1}) is of the same order than the one measured on MA-based perovskite materials. This shows that the thermal properties of such materials are almost

the same whatever the nature of the cation. Therefore, the recently observed enhanced thermal stability of these triple-cation perovskites cannot be explained by a different value of their thermal conductivity or thermal diffusivity. The enhanced thermal stability of these perovskites may rather come from a chemical origin.

Supplementary material

See supplementary material for details regarding the synthesis of the mixed-cation perovskite material [$Cs_{0.05(}(FA_{0.83}MA_{0.17})_{0.95}Pb(I_{0.83}Br_{0.17})_3$], for the SEM, EDX and XRD characterization of the layers.

Acknowledgments

SEM characterizations performed were supported by the region Île-de-France in the framework of DIM Nano-K. Z.H. acknowledges the China scholarship council (CSC) for Ph.D. thesis scholarship. We acknowledge the project “PROCES” (ANR-17-CEO5-0028-01).

References

[1]J.-P. Correa-Baena, A. Abate, M. Saliba, W. Tress, T. Jesper Jacobsson, M. Grätzel, and A. Hagfeldt, Energy Environ. Sci. 10 (3), 710 (2017).

[2]W.S. Yang, J.H. Noh, N.J. Jeon, Y.C. Kim, S. Ryu, J. Seo, S.I. Seok, Science 348 (6240), 1234 (2015).

[3]J. H. Noh, and S. I. Seok, MRS Bulletin, 40(8), 648 (2015) .

[4]W. S. Yang, B.-W. Park, E. H. Jung, N. J. Jeon, Y. C. Kim, D. U. Lee, S. S. Shin, J. Seo, E. K. Kim, J. H. Noh, S. I. Seok, Science 356(6345), 1376 (2017).

[5]D. Yang, R. Yang, K. Wang, C. Wu, X. Zhu, J. Feng, X. Ren, G. Fang, S. Priya, and S. (Frank) Liu, Nature Communications 9, 3239 (2018).

[6]F. Sahli, J. Werner, B. A. Kamino, M. Bräuninger, R. Monnard, B. Paviet-Salomon, L. Barraud, L. Ding, J. J. Diaz Leon, D. Sacchetto, G. Cattaneo, M. Despeisse, M. Boccard, S. Nicolay, Q. Jeangros, B. Niesen, and C. Ballif, Nature Materials 17, 820 (2018).

[7]A. Extance, "Perovskites on trial", Nature 570, 429 (2019).

[8]D. P. McMeekin, G. Sadoughi, W. Rehman, G. E. Eperon, M. Saliba, M. T. Hörantner, A. Haghighirad, N. Sakai, L. Korte, B. Rech, M. B. Johnston, L.M. Herz, H.J. Snaith, Science 351(6269), 151 (2016).

[9]Z. Wang, Q. Lin, F. P. Chmiel, N. Sakai, L. M. Herz, and H. J. Snaith, Nature Energy 2, 17135 (2017).

[10]T.A. Berhe, W.-N. Su, C.-H. Chen, C.-J. Pan, J.-H. Cheng, H.-M. Chen, M.-C. Tsai, L.-Y. Chen, A. A. Dubale, and B.-J. Hwang, Energy Environ. Sci. 9, 323 (2016).

[11]A. T. Ava, A.A. Mamun, S. Marsillac, and G. Namkoong, Appl. Sci. 9, 188 (2019).

[12]J. Cao, S. X. Tao, P. A. Bobbert, C.-P. Wong, and N. Zhao, Adv.Mater. 30, 1707350 (2018).

[13]W. S. Yang, J. H. Noh, N. J. Jeon, Y. C. Kim, S. Ryu, J. Seo, and S. I. Seok, Science 348(6240), 123412 (2015).

[14]C. Frétigny, J. P. Roger, V. Reita, and D. Fournier, J. Appl. Phys. 102, 116104 (2007).

[15]F. Xu, C. Frétigny, D. Fournier, L. Belliard, S. Vincent, B. Perrin, S. Martin, C. Secouard, J.-Y. Duquesne, J. Appl. Phys. 113, 244304 (2013).

[16]D. Jimenez-Olarte, O. Vigil-Galan, J. de la Rosa, D. Seuret-Jim´enez, and G. Contreras-Puente, Revista Mexicana de Fisica 61, 160 (2015).

[17]C. Hudaya, B. J. Jeon, and J. K. Lee, ACS Appl. Mater. Interfaces 7(1), 57 (2015).

[18]E. A. Scott, J. T. Gaskins, S. W. King, and P. E. Hopkins, APL Materials 6, 058302 (2018).

[19]D. J. Kim, D. S. Kim, S. Cho, S. W. Kim, S. H. Lee, J. C. Kim, International Journal of Thermophysics 25(1), 281 (2004).

[20]A. Pisoni, J. Jaćimović, O.S. Barišić, M. Spina, R. Gaál, L. Forró, and E. Horváth, J. Phys. Chem. Lett. 5(14), 2488 (2014).

[21]Z. Guo, S. J. Yoon, J. S. Manser, P. V. Kamat, and T. Luo, J. Phys. Chem. C 120(12), 6394 (2016).

[22]R. Heiderhoff, T. Haeger, N. Pourdavoud, T. Hu, M. Al-Khafaji, A. Mayer, Y. Chen, H.-C. Scheer, and T. Riedl, J. Phys. Chem. C 121, 28306 (2017).

[23]Q. Chen, C. Zhang, M. Zhu, S. Liu, M.E. Siemens, S. Gu, J. Zhu, J. Chen, X. Wu, C. Liao, J. Zhang, X. Wang, and M. Xiao, Appl. Phys. Lett. 108, 081902 (2016)

[24]A. Kovalsky, L. Wang, G.T. Marek, C. Burda, and J.S. Dyck, J. Phys. Chem C 121, 3228 (2017).

[25]A. Kovalsky, L. Wang, X. Guo, J. S. Dyck, and C. Burda, J. Phys. Chem C 122, 13243 (2018).

[26]Y. Wang, R. Lin, P. Zhu, Q. Zheng, D. Li, and J. Zhu, Nano Lett. 18, 2772 (2018).

[27]M. Wang, and S. Lin, Advanced Functional Materials, 26, 5297 (2016).

[28]C.C. Stoumpos, C.D. Malliakas, and M.G. Kanatzidis, Inorg. Chem. 52, 9019 (2013).

[29]N. Onoda-Yamamuro, T. Matsuo, and H. Suga, J. Phys. Chem. Solids, 51(12), 1383 (1990).